Desalination and Water Treatment
www.deswater.com
doi: 10.1080/19443994.2015.1048738

57 (2016) 12019–12036
June

Taylor & Francis
Taylor & Francis Group

Assessing the performance of solar desalination system to approach near-ZLD under hyper arid environment

Ahmed F. Mashaly[a,*], A.A. Alazba[a,b], A.M. Al-Awaadh[b]

[a]*Alamoudi Chair for Water Researches, King Saud University, P.O. Box 2460, Riyadh 11451, Saudi Arabia, Tel. +966 1 467 3737; Fax: +966 1 467 3739; emails: amashaly@ksu.edu.sa, mashaly.ahmed@gmail.com (A.F. Mashaly), Tel. +966 1 467 8382; email: alazba@ksu.edu.sa (A.A. Alazba)*
[b]*Agricultural Engineering Department, King Saud University, P.O. Box 2460, Riyadh 11451, Saudi Arabia, Tel. +966 1 467 7582; email: assiry@ksu.edu.sa*

Received 15 September 2014; Accepted 3 May 2015

ABSTRACT

The aim of this study was to investigate the performance of a solar desalination system using three different types of feedwater to reach near zero liquid discharge (ZLD) under hyper arid environment. Solar still was used to desalinate seawater (SW), groundwater (GW), and agricultural drainage water (DW). The influence of meteorological parameters on the performance of the solar still was investigated. The system productivity (MD), operational recovery ratio (ORR), and thermal efficiency (η_{th}) were determined during the desalination process. Some physicochemical properties of the feed, brine, and distilled water were measured such as total dissolved solids (TDS), electrical conductivity (EC), pH, density (ρ), and color. The performance was in direct proportion to solar radiation and ultraviolet index. The average ranges of the MD, ORR, and η_{th} were 0.56 L/m^2/h, 36.77, and 52.38%, respectively, for all waters. The final recovery ratios were 68, 93, and 95.6% for SW, GW, and DW, respectively. Statistical empirical models were found to predict the system performance with a range of R^2 was 88–96%. One major output of this research is the assessment of the solar still system during the desalination process for near-ZLD, which adds a new perspective to system design, analysis, and modeling of the possible use of solar energy in ZLD desalination process. On the other hand, more studies are required for the continuous pilot production system, modeling for commercial production, in addition to full economic evaluation of the system.

Keywords: Solar desalination; Solar still; Zero liquid discharge; Recovery ratio

1. Introduction

Worldwide, only two-thirds of the population has access to pure and potable water [1]. The lack of pure and potable water is a critical problem that is constantly increasing, pursuant to population growth and changes in weather conditions. Presently, the global demand for water also is increasing as is environmental pollution from fossil fuels, and the lack of nonrenewable resources and economic crises increase the utilization of renewable energy, such as solar [2–8]. It has been reported that owing to water inadequacies for the growing global population and the need to maintain the environment, the zero liquid discharge

*Corresponding author.

(ZLD) method has been under consideration and focus [9]. The ZLD method is considered an important approach to manage water resources, maximize water savings, decrease desalination and water treatment costs, and conserve water resources and the environment [9]. Farahbod et al. [10] stated that desalination based on the ZLD process is the best and most logical solution to reduce or remove the biological problems that result from concentrated, brine wastewater drainage into the ecosystem. The aim of the ZLD process considers two serious environmental issues for desalination plants: reusing the concentrated brine effluent from desalination units, thus negating the need for disposal (zero discharge) and producing potable water and salt. The ZLD process is the most promising technique for solving these problems [9–11]. In other words, the ZLD approach results in the cost-effective concentrating of the brine near complete dryness. The removed water can be recycled to increase its recovery ratio. The remaining, reduced volume waste is a dry or semi-dry solid that should be disposed of in special sites [9] or further processed for production of salts [12].

Desalination based on ZLD technique can be implemented in several ways. Stanford et al. [13] mentioned that with energy costs persistently increasing and carbon emission concerns escalating, the future of desalination will rely on continued developments in decreasing energy requirements. García-Rodríguez [14] reported that using renewable energies such as solar energy for desalination is suitable, especially in rural and remote areas where conventional energy supply and skilled workers are not usually available. The solar desalination process is an environmental-friendly and cost-saving process that is competitive with other desalination techniques [15–19]. The solar energy can be used directly or indirectly for desalination. The direct process exploits solar energy to produce distillate directly in the solar collector, while in the indirect collection systems, two sub-systems are used; one for solar energy collection and the other for producing distillate water [10]. The direct solar desalination is essentially suited for small production systems, such as solar stills. In the area of solar desalination, Ayoub and Malaeb [20] mentioned that there is a need to develop solar stills into a more efficient technology for sustainable water production. Solar stills can be the best solution to supply water to arid and remote regions without relying on high-technology and skills [21], since it requires low operation and maintenance cost but need large areas and high initial costs [22]. The idea of solar stills is similar to the natural hydrological cycle that involves two processes, namely evaporation and condensation [23]. Simply, it comprises a transparently roofed basin containing the sea-, waste-, or brackish water to be evaporated. The water, heated through solar radiation, evaporates and condenses as it hits the transparent cooler cover and drips down into a channel as distillate water [20].

The majority of existing research in solar desalination has concentrated on modifying the solar still design to present components that would allow water to either evaporate or condense faster [24]. Moustafa et al. [25] conducted experimental investigations on stepped solar still and wick-type evaporator still, and the efficiency of the still improved by decreasing the radiation losses from the basin. Zurigat and Abu-Arabi [26] used and studied double glass cover. Dimri et al. [27] conducted theoretical and experimental analyses of a solar still using a flat plate collector with various condensing materials. Moreover, many studies have focused on different designs of solar stills, by way of example, not exhaustive enumeration, simple solar still [28], single basin solar still [29], double basin solar still [30], triple basin solar still [31], multiple basin [32], tubular solar still [33], wick-type solar still [34], triangular solar still [35], and hemispherical solar still [36]. The aim of the multiplicity of designs is to attempt to improve and optimize overall solar still performance. With regard to solar distillation/desalination with ZLD technique, there are some published papers. Madani [37] proposed a ZLD direct contact freezing/solar evaporator desalination complex as an efficient system to decrease the environmental impact of concentrated brine from seawater (SW) desalination plants. Additionally, an advanced solar dryer was investigated to promote brine concentration and/or ultimate salt recovery from the multiple-effect distillation (MED) brine effluent, accordingly contributing to the production of salt, adding one more valuable output to the entire system and enhancing the economics and the environmental performance of an MED desalination plant [38]. Assiry [12] noted that solar evaporation ponds are particularly appropriate to dispose of rejected brine from inland desalination plants in arid and semi-arid areas owing to the abundance of solar energy. Farahbod et al. [39] stated that the ZLD desalination process is the most promising technology to prevent salinity and thermal shocks to the ecosystem through effluent streams of desalination unit drained into the sea. Generally short, solar stills have many advantages: simplicity of design, low installation cost, independent water production, and easy maintenance [22]. Furthermore, they can be employed as one solar desalination unit in near-ZLD or ZLD desalination process. Assiry [12] applied the ohmic heating technique to approach near-ZLD. The study revealed

that applying the ohmic heating technique can approach recovery, but in cost or energy where the ranges of the recovery rate and specific energy were 81–93.5% and 4,550–5,071 kJ/kg, respectively. From this standpoint, we can realize that reaching near-ZLD requires high energy and high cost, and this will certainly vanish if we use solar energy as an energy source. In this study, a solar still/panel (F Cubed. Ltd., Carocell Solar Panel. Australia) was used in the experiments. This system has been used for desalination in different locations in the world such as Australia, Bangladesh, Indonesia, Philippines, Vietnam, India, and Myanmar (F Cubed. Ltd., Australia), but has not been investigated, tested, and evaluated to reach near-ZLD under hyper arid environment. Therefore, the objective of this study was to investigate the performance and capacity of the solar desalination system using three different types of quality water inputs to reach near ZLD under hyper arid environment.

2. Materials and methods

2.1. Experiment setup, instrumentation, and measurements

The experiments were conducted at the agricultural research and experiment station at the Department of Agricultural Engineering, King Saud University, Riyadh, Saudi Arabia (24˚44′10.90′′N, 46˚37′13.77′′E) between February and November 2013. The weather data were obtained from a weather station (model: Vantage Pro2, manufacturer: Davis, USA) close by the experimental site (24˚44′12.15′′N, 46˚37′ 14.97′′E). The solar still system used in the experiments was constructed from a 6 m^2 single stage C6000 panel (F Cubed. Ltd., Carocell Solar Panel. Australia). The solar-still panel was manufactured using modern, cost-effective materials such as coated polycarbonate plastic. When heated, the panel distilled a film of water that flowed over the absorber mat of the panel. The panel was fixed at an angle of 29^o from the horizontal plane. The basic construction materials are galvanized steel legs, aluminum frame, and polycarbonate covers. The transparent polycarbonate was coated on the inside with a special material to prevent fogging (patent for F Cubed- Australia). Front and cross-sectional views of the solar still are presented in Fig. 1. The water was fed to the panel using a centrifugal pump (model: PKm 60, 0.5 HP, Pedrollo, Italy) with a constant flow rate of 10.74 L/h. The fed water was supplied by eight drippers/ nozzles, creating a film of water that flowed over the absorbent mat. Underneath the absorbent mat, there was an aluminum screen that helped to distribute the water across the mat. Beneath the aluminum screen was an aluminum plate. Aluminum was chosen for its hydrophilic properties, to assist in the even distribution of the sprayed water. Water flowed through and over the absorbent mat, where solar energy was absorbed and partially collected inside the panel; as a result, the water was heated and evaporated as the hot air circulated naturally within the panel. The hot air carrying the vapor flowed toward the top of the panel, then reversed its direction to approach the bottom of the panel. During this process of circulation, the humid air touched the cold surfaces of the transparent polycarbonate cover and the bottom polycarbonate layer, so that the vapor condensed. The condensed water flowed down on the cover of the panel and was collected in the form of a distilled stream.

Three feed-water sources were used as inputs to the system: SW, groundwater (GW), and agricultural drainage water (DW). Raw SW was obtained from the Gulf, Dammam, in eastern Saudi Arabia (26˚26′24.19′′ N, 50˚10′20.38′′ E). Raw groundwater, a reject product of groundwater treatment plants, was obtained from Bouwaib Station, east of Riyadh, the capital of Saudi Arabia (25˚ 6′58.36′′N, 46˚50′28.49′′E). Raw agricultural DW was obtained from Al-Oyun City, Al-Ahsa, in eastern Saudi Arabia (25˚35′7.02′′N, 49˚35′48.17′′E). The initial concentrations of total dissolved solids (TDS) in the three types of water, along with their pH, density (ρ), and electrical conductivity (EC), are listed in Table 1. The three inputs were fed separately to the panel using the pump described above. The residence time—the time taken for the water to pass through the panel—was approximately 20 min. Consequently, samples of feedwater, distilled water, and brine water were taken every 20 min. The flow rate for feedwater, distilled water, and brine water were measured every 20 min. Moreover, the temperatures at the geometric center of the feedwater inlet, brine water outlet, and distilled water outlet were continuously measured. A simple sketch of the solar desalination system is displayed in Fig. 2.

The temperatures of the feedwater (T_F), brine water (T_B), and distilled water (T_D) were measured with a calibrated T-Type copper constant, Teflon coated thermocouple, ±1.5˚C accuracy (Omega Instrument). Temperature data for the feed, brine, and distilled water were recorded on a data logger (model: 177-T4, Testo, Inc., UK) at 1 min intervals. The amount of feedwater measured by calibrated digital flow meter was mounted on the feedwater line (micro-flo, Blue-White, USA). The amounts of brine water and distilled water were measured by graduated cylinder. Special quality parameters were measured for the feed, brine, and distilled streams such as The TDS, EC, power of hydrogen (pH), density (ρ), and Color components

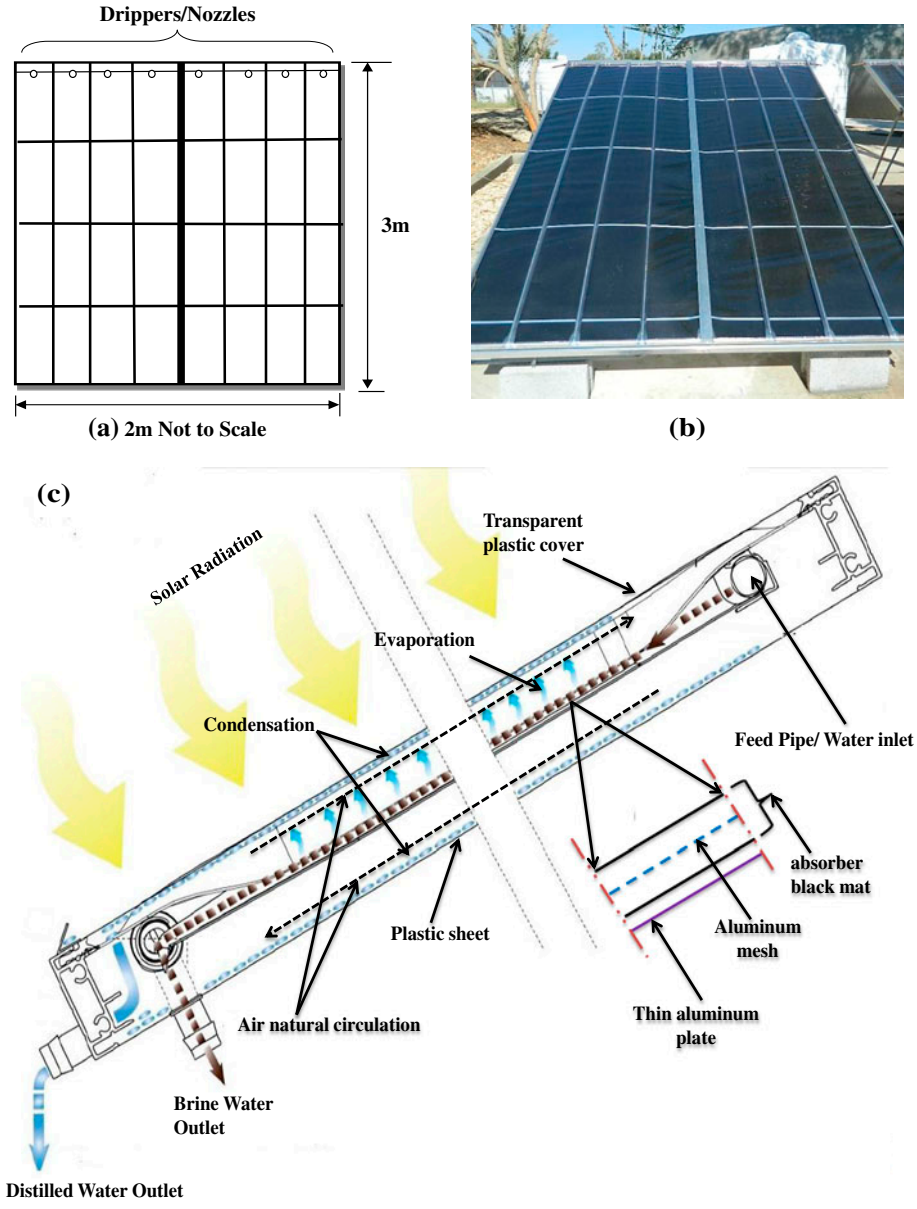

Fig. 1. Solar still panel: front section (a), picture of the panel (b), and cross-sectional view of the solar still panel (c).

Table 1
Some properties of the SW, GW, and agricultural DW used for desalination process

Property	SW	GW	DW
TDS (PPT)	41.1	7.45	4.71
pH	8.02	8.1	8.1
ρ (g cm^{-3})	1.04	1.01	1.001
EC (mS cm^{-1})	66.34	11.93	7.54

(L^*, a^* and b^*). The TDS and EC of feed, brine, and distilled water were checked using calibrated TDS meter (Cole-Parmer Instrument, Vernon Hills, USA). A pH meter, (model: 3510 pH meter, Jenway, UK) was used to measure pH of the samples. A digital-density meter (model: DMA 35 $_N$, Anton Paar, USA) was used to measure ρ. Color components were measured using Colorflex (HunterLab-ColorFlex, Hunter Associates Laboratory, Inc.-Reston, US). A sample of 27 ml was poured into the sample cup and then the cup was covered and inserted into the measuring chamber. Color components were measured where L^* is the lightness or darkness, (black, $L^* = 0$; white, $L^* = 100$), $+a^*$ is redness, $-a^*$ is greenness, $+b^*$ is yellowness, and $-b^*$ is blueness. This instrument was calibrated with standard calibration plates provided by the manufacturer.

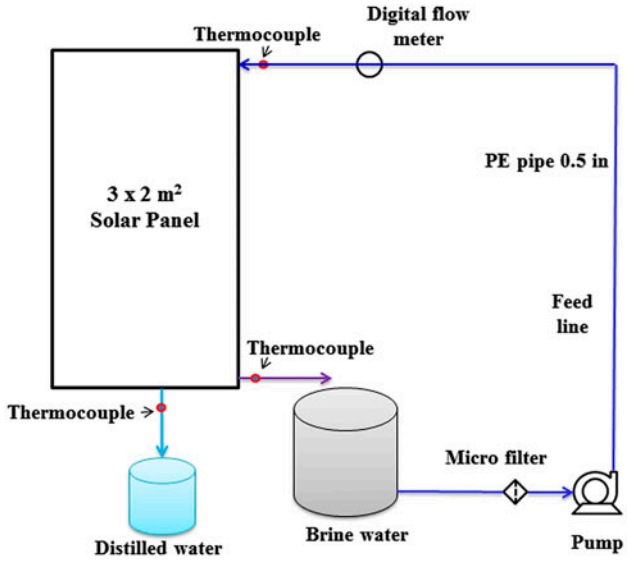

Fig. 2. Simple sketch of the experiment setup.

The weather data, such as air temperature (T_o), relative humidity (RH), wind speed (U), solar radiation (R_s), and ultra violet index (UVI), were obtained from a weather station mentioned above. The productivity capacity or the amount of distilled water produced by the system in a given time, was obtained by collecting and measuring the amount of water cumulatively produced over time. The operational recovery ratio (ORR) is defined as the mass ratio of the distilled water produced per unit mass of feedwater using the following equation [40]:

$$\mathrm{ORR} = \frac{\mathrm{MD}}{\mathrm{MF}} \times 100 \quad (1)$$

where MD: is the mass of distilled water collected during a certain period, kg, MF: is the mass of feedwater during the same period, kg The instantaneous thermal efficiency (η_{th}) of the system during a certain period can be calculated using the following equation [41]:

$$\eta_{th} = \frac{\mathrm{MD} \times L}{R_S \times A} \times 100 \quad (2)$$

where, MD is the mass flow rate of distilled water collected during this period, kg/s L: Latent heat of vaporization = 2275 kJ/kg, R_s: Solar radiation on tilted surface, kW/m^2A: Area of solar still, m^2.

All statistical analysis and data processing in this research were carried out using IBM's Statistical Package for the Social Sciences Statistics 21 (SPSS Inc., Chicago, IL, USA). In the experiment, there were three dependent variables (the MD, ORR, and η_{th} of solar-desalination system) and nine independent variables (T_o, RH, U, R_s, UVI,TDS$_F$, TDS$_B$,T_F, and T_B). MD, ORR, and η_{th} were predicted using models obtained from the regression analysis (stepwise method) of solar-desalination experiments using meteorological and operational parameters.

3. Results and discussion

3.1. Solar desalination system performance

For SW, the system was operated during the period from 23/02/2013 to 23/04/2013, the data obtained can be averaged on an hourly basis. A sample of the meteorological and operational data was shown in Table 2. Generally, the range of T_o, RH, U, R_s, UVI, T_F, T_B, TDS$_F$, and TDS$_B$ were 17.7–32.9 (°C), 13.00–67.25 (%), 0.05–12.09 (km/h), 144.22–905.35 (W/m^2), 0.11–5.83, 24.32–42.23 (°C), 32.76–67.87 (°C), 41.60–129.73 (PPT), and 47.13–132.57 (PPT), respectively. The hourly ranges of MD, ORR, and η_{th} were 0.15–0.94 (L/m^2/h), 7.13–65.77 (%), and 20.65–80.88 (%), respectively. Histograms for the minimum, average and maximum MD, ORR, and η_{th} for the SW desalination process were showed in Fig. 3. From this figure, the overall averages during the whole days were 0.53 L/m^2/h, 30.09, and 53.53% for MD, ORR, and $\eta_{th,}$ respectively. Moreover, it was cleared from the figure that the efficiency decreased on the last day of the operation, which may be due to the presence of clouds. Furthermore, by correlating meteorological and operational parameters with MD, ORR, and η_{th}, it was found that MD and ORR were the most affected by R_s and UVI where, the correlation coefficient (R) ≥ 0.70, whereas η_{th} was mainly dependent on TDS$_{F,}$ as indicated in the correlation Table 3. Also, a typical example of the most affected parameters of the independent variables, with $R \geq 0.70$ during one day of operation with SW was presented in Fig. 4, which shows the relationship between the dependent parameters and the independent parameters with the highest R. In this figure, the change of R_s, UVI, and MD during one day of operation was illustrated. It was evident that the MD increased as the R_s and UVI increased and the maximum MD ≥ 0.8 L/m^2/h occurred in the mid of the day, where the R_s and UVI were around 700 W/m^2 and 4.5, respectively. In Fig. 4, the highest ORR was 35.15% occurred around the mid of the day (from 10 to 12:30) when the R_s was 717.62 W/m^2 and UVI was 4.30. The change of the η_{th} and the TDS$_F$ was presented in Fig. 4. The highest η_{th} during this particular day was

Table 2
Sample of weather and operational parameters of the desalination process for one day

Date	Time	T_o (°C)	RH (%)	U (km/h)	R_s (W/m^2)	UVI (–)	T_F (°C)	T_B (°C)	TDS_F (PPT)	TDS_B (PPT)	ORR (%)	η_{th} (%)	MD (L/m^2/h)
SW													
24/02/2013	9 AM	22.00	18.57	5.28	528.33	2.40	33.83	44.88	48.20	59.40	24.63	68.75	0.58
	10 AM	23.58	17.21	6.57	656.94	3.60	35.56	47.73	48.87	64.93	32.20	71.49	0.75
	11 AM	24.86	16.08	7.18	717.62	4.30	36.87	49.65	49.90	69.50	35.15	70.95	0.81
	12 PM	26.25	13.25	7.14	713.95	4.19	37.86	49.61	51.13	70.67	34.19	68.51	0.78
	1 PM	26.79	13.00	6.33	632.75	3.30	38.56	48.52	52.30	68.13	28.10	63.35	0.64
	2 PM	26.93	13.46	4.91	490.68	1.98	38.38	44.96	53.47	63.60	19.51	55.81	0.44
	3 PM	26.45	14.00	3.12	311.57	0.88	37.18	38.82	54.27	58.83	9.58	43.04	0.21
GW													
31/05/2013	9 AM	35.91	8.53	7.21	720.55	4.54	43.27	52.52	7.48	10.74	44.91	58.95	0.68
	10 AM	37.34	7.02	8.44	843.79	6.29	44.96	56.36	7.61	12.91	56.63	61.43	0.83
	11 AM	38.28	6.35	8.99	899.49	7.27	46.30	56.78	7.73	14.71	61.34	61.69	0.89
	12 PM	39.66	5.49	8.96	896.25	7.13	47.58	56.77	7.84	14.79	58.78	59.34	0.85
	1 PM	40.91	4.94	8.28	828.16	5.90	49.24	56.80	8.07	13.94	53.28	57.26	0.76
	2 PM	41.63	4.29	6.97	696.79	4.03	50.44	53.03	8.21	12.05	42.31	53.15	0.59
	3 PM	41.16	4.44	5.11	511.44	2.19	49.19	48.77	8.27	9.76	23.16	36.95	0.31
DW													
08/10/2013	9 AM	29.26	16.62	4.88	488.48	2.16	33.86	45.96	13.90	11.01	25.34	40.32	0.31
	10 AM	26.21	17.32	7.19	719.44	4.13	34.55	48.69	18.38	26.50	44.02	54.45	0.63
	11 AM	27.75	14.78	7.83	783.02	4.83	36.00	49.77	19.07	30.23	47.64	54.58	0.68
	12 PM	29.34	12.98	7.71	771.17	4.56	36.97	50.99	19.96	31.87	45.42	52.82	0.65
	1 PM	30.33	12.27	6.86	686.22	3.44	37.69	49.61	21.23	31.80	36.67	47.66	0.52
	2 PM	30.76	11.98	5.37	536.68	2.06	37.26	47.24	22.37	30.04	25.69	41.70	0.36
	3 PM	38.98	9.51	3.45	345.06	1.13	41.89	45.95	22.90	29.57	18.00	38.00	0.20

71.49%, reached at about 10 AM The TDS_F increased from 47 (PPT) to above 54 (PPT) by the end of the operation at 3 PM. Overall with SW, the desalination water system was able to approach a total recovery ratio of 68%, beyond this ratio, a mixing between the distilled stream and the brine stream occurred. This mixing problem might be due to salt crystal formation; so, a modification of the system design is necessary to approach near ZLD.

Furthermore, for GW, the system was run during the period from 31/05/2013 to 20/09/2013, the data obtained was averaged based on an hourly basis. A sample of the meteorological and operational data was shown in Table 2. Through the entire period of the experiment, the ranges of T_o, RH, U, R_s, UVI, T_F, T_B, TDS_F, and TDS_B were 35.24–43.36 (°C), 2.57– 11.52 (%), 0.00–7.20 (km/h), 339.57–899.49 (W/m^2), 1.09–7.27, 40.80–51.05 (°C), 42.42–63.41(°C), 7.48–107.38 (PPT), and 8.27–108.34 (PPT), respectively. Also, the range of MD, ORR, and η_{th} were 0.15–0.89 (L/m^2/h), 11.75–64.61 (%), and 23.70–61.69 (%), respectively. The histograms in Fig. 5 represent MD, ORR, and η_{th} at their minimum, average, and maximum values. From this figure, the general averages during the total days were 0.59 L/m^2/h, 43.08, and 49.64% for MD, ORR, and η_{th}, respectively. By correlating weather and operational parameters with MD, ORR, and η_{th}, it was found that MD, ORR and η_{th} were dependent on R_s and UVI as illustrated in the correlation Table 3 with $R \geq 0.90$. A typical example of one day operation can be seen in Fig. 6. From this figure, the averages of R_s and UVI were 770.93 W/m^2 and 5.33, respectively. Additionally, it is noted that the increase in R_s and UVI increases each of MD, ORR, and η_{th}. Also, η_{th} values were close to a large extent throughout the day. However, the solar still system with GW was able to approach final recovery ratio of 93%, beyond this ratio, a mixing between the distilled stream and the brine stream occurred. This mixing problem might be because of the formation of salt crystals. Thus, it is recommended to modify the still system design to overcome this problem.

Moreover, for DW, the system was run during the period from 05/10/2013 to 01/11/2013. The obtained data were averaged based on one hour operation. Also, a sample of the meteorological and operational data was presented in Table 2. The ranges of T_o, RH, U, R_s, and UVI were 26.21–38.98 (°C), 8.03–29.30 (%), 0.08–7.83 (km/h), 345.06–799.11 (W/m^2), 1.13–5.44, respectively. The ranges of the

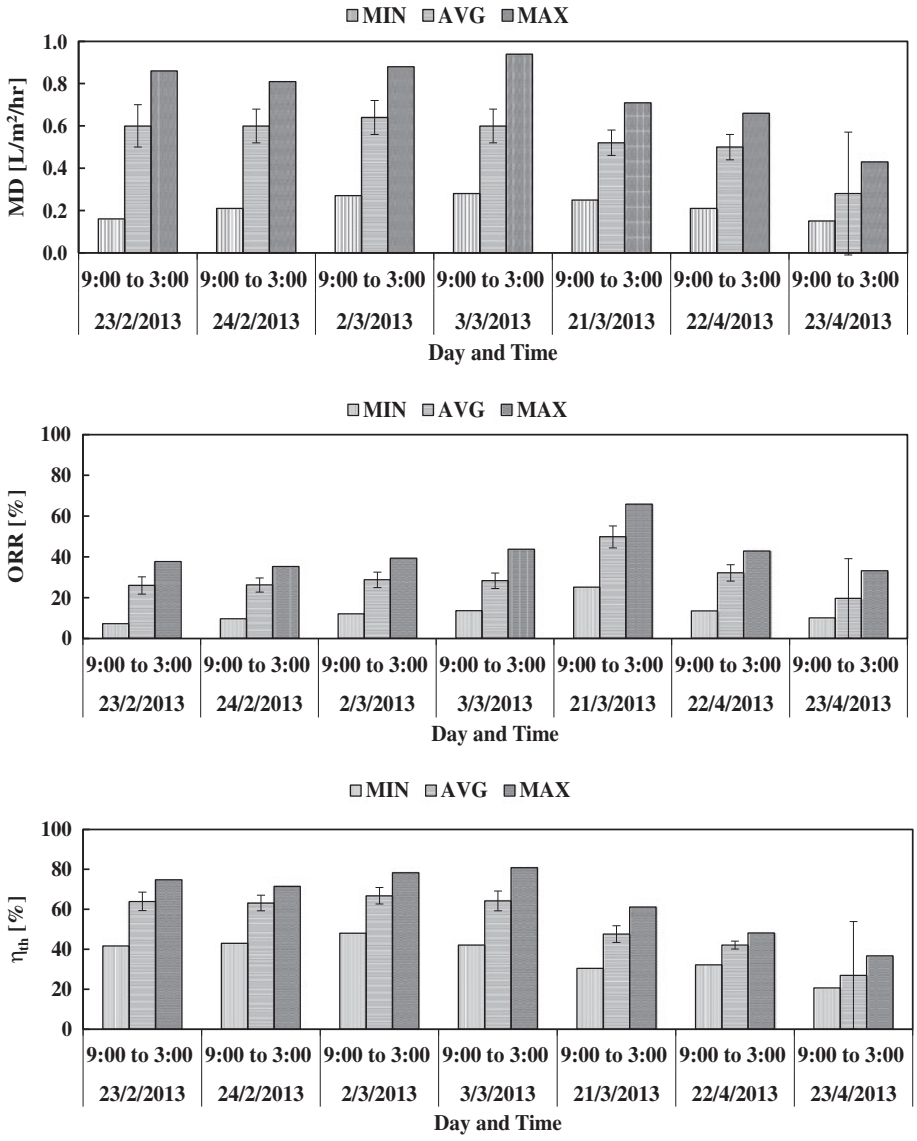

Fig. 3. Histograms for the MIN, AVG, and MAX of MD and ORR and η_{th} for the SW desalination process. The vertical error bar represents the standard deviation.

process variables, namely T_F, T_B, TDS_F, and TDS_B were 33.86–42.59 (°C), 45.95–53.60 (°C), 4.74–96.47 (PPT), and 7.80–107.45 (PPT), respectively. Furthermore, the hourly ranges of MD, ORR, and η_{th} were 0.26–0.86 (L/m^2/h), 18.00–72.63 (%), and 34.00–68.09 (%), respectively. The histograms in Fig. 7 showed the minimum, average, and maximum values of the MD, ORR, and η_{th}. It was noted from this figure that the averages of MD, ORR, and η_{th} during the operation days were 0.54 L/m^2/h, 39.95, and 52.87%, respectively. Also, by the same way as with the previous two types of water, the weather and operational parameters were correlated with MD, ORR, and η_{th}. It was found that MD, ORR were dependent on R_s and UVI as showed in the correlation Table 3. On the other hand, η_{th} was dependent on T_B. Additionally, a typical example of the most affected parameters by the independent variables with $R \geq 0.70$ during one day of operation were presented in Fig. 8. Moreover, the solar desalination system with DW was capable of approach total recovery ratio 95.6%, beyond this ratio, a mixing between the distilled stream and the brine stream occurred. This mixing problem might be due to the formation of salt crystals. Hence, a modification of the system design is necessary to get over this problem.

Table 3
The correlation values (R) between dependent parameters MD, ORR, and η_{th} and independent parameters

Parameter		T_o (°C)	RH (%)	U (km/h)	R_S (W/m^2)	UVI (–)	T_F (°C)	T_B (°C)	TDS_F (PPT)	TDS_B (PPT)
SW										
MD	(L/m^2/h)	−0.08	0.01	−0.31	0.72	0.73	−0.07	0.37	−0.42	−0.17
ORR	(%)	−0.38	0.55	−0.13	0.82	0.83	−0.42	0.61	0.03	0.35
η_{th}	(%)	−0.04	−0.10	−0.57	0.28	0.29	−0.06	−0.06	−0.77	−0.58
GW										
MD	(L/m^2/h)	−0.45	0.13	−0.02	0.98	0.97	−0.29	0.63	−0.40	−0.27
ORR	(%)	−0.40	0.05	0.04	0.98	0.97	−0.27	0.58	−0.41	−0.28
η_{th}	(%)	−0.51	0.15	−0.05	0.94	0.90	−0.33	0.68	−0.45	−0.31
DW										
MD	(L/m^2/h)	0.07	0.08	−0.11	0.90	0.93	0.11	0.62	0.04	0.13
ORR	(%)	0.20	0.10	−0.23	0.83	0.89	0.21	0.57	−0.01	0.06
η_{th}	(%)	0.29	0.27	−0.42	0.49	0.57	0.26	0.71	0.38	0.41

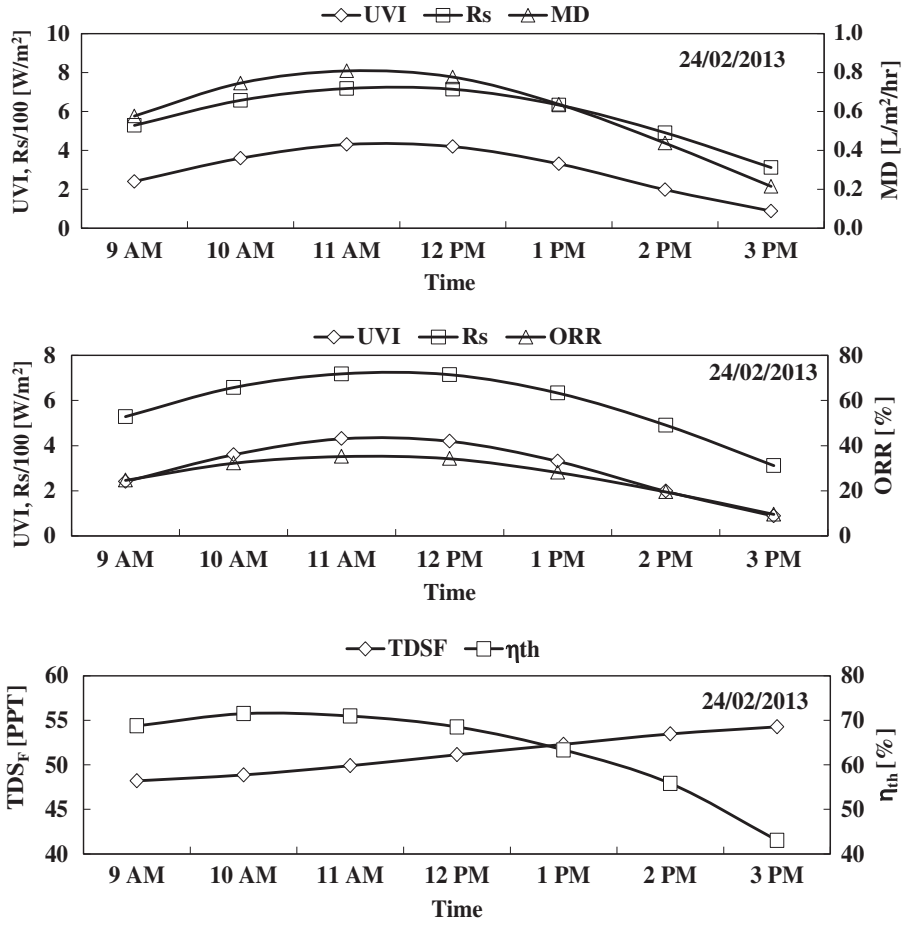

Fig. 4. Typical example of the changes of MD, ORR, and η_{th} during one day of operation for SW.

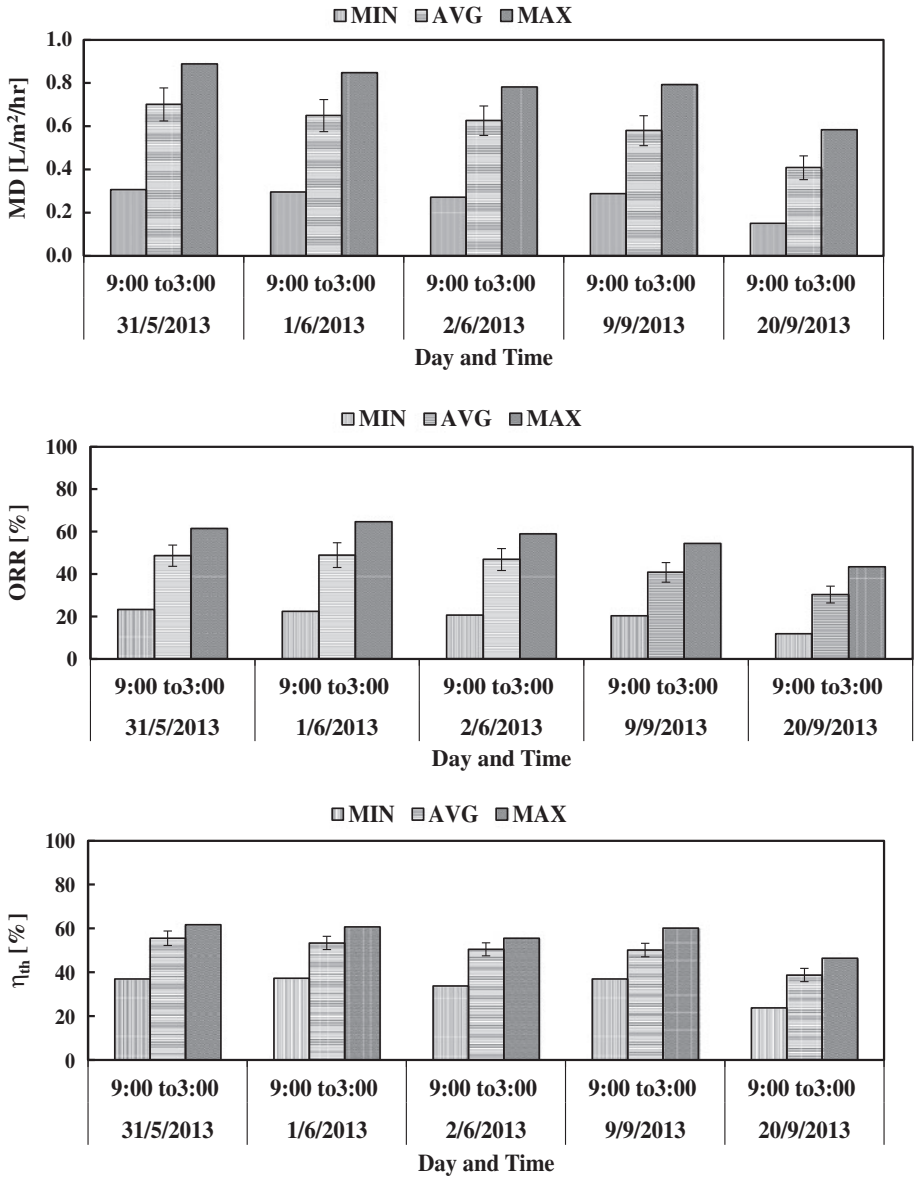

Fig. 5. Histograms for the MIN, AVG, and MAX of MD and ORR and η_{th} for the GW desalination process. The vertical error bar represents the standard deviation.

3.2. Total system performance

The overall performance of the solar-desalination system was as follows. The average MD for the three types of water was 0.55 $L/m^2/h$ (5 $L/m^2/d$). This is consistent with the findings of Kabeel et al. [42] and Radhwan [43]. The average ORR and η_{th} were 37.1 and 52%, respectively. Fig. 9 displays the hourly average of MD, ORR, and η_{th} for each operation day for each type of water. It was obvious from the figure that the performance in the middle of the day was higher than that in the beginning and the end of the day. Also, it was found that the average overall performance with GW type was greater than that with other water types. This may be due to the run-time which was at the end of spring and the end of the summer. This time of the year enjoys good climatic conditions and abundant solar radiation which equal to 730 W/m^2 as an average. A fluctuation in efficiency was a result of changing weather conditions throughout the day. Moreover, the average final recovery ratio for the three types of water was 86%.

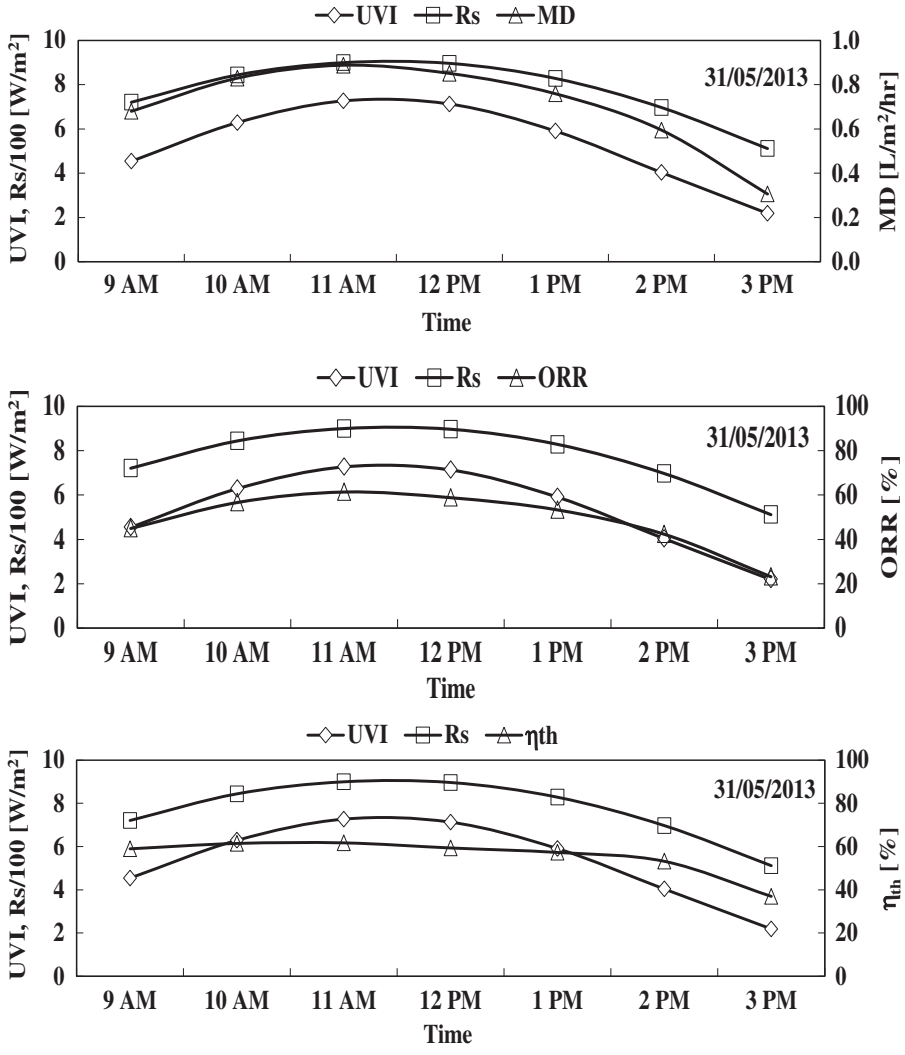

Fig. 6. Typical example of the changes of MD, ORR, and η_{th} with R_s and UVI during one day of operation for GW.

3.3. Statistical Analysis of the parameters of the solar desalination process

The effect of the T_o (°C), RH (%), U (km/h), R_s (W/m^2), UVI, T_F (°C), T_B (°C), TDS_F (PPT), TDS_B (PPT), and their interactions on the MD (L/m^2/h), ORR (%), and η_{th} (%), were statistically analyzed. The nonlinear regression analysis (stepwise method) was applied to find a reasonable set of empirical equations with significant constants. With SW, the obtained models were shown in Eqs. (3)–(5) with R^2 equal to 0.91, 0.94, and 0.88 for MD, ORR, and η_{th}, respectively.

$$\mathrm{MD} = 0.126 + 0.243(\mathrm{UVI}) - 2.2 \times 10^{-5}(\mathrm{TDS_F})^2 - 0.018(\mathrm{UVI})^2 - 0.003(U \times \mathrm{UVI}) \quad (3)$$

$$\mathrm{ORR} = -4.433 + 0.119(\mathrm{RH.UVI}) + 0.044(R_S) - 0.010(U \times \mathrm{TDS_F}) \quad (4)$$

$$\eta_{th} = 13.992 - 0.007(\mathrm{TDS_F^2}) + 20.99(\mathrm{UVI}) - 0.017(R_s \times \mathrm{UVI}) + 0.82(\mathrm{TDS_F}) - 0.002(\mathrm{RH} \times \mathrm{TDS_F}) \quad (5)$$

where the applicability of these equations were limited within the following ranges of the independent variables: RH: 12.90–70%; U: 0–12.65 km/h; R_s: 75.10–920.69 W/m^2; UVI: 0–6 and TDS_F: 41.4–130 PPT. These models have shown the significance of all individual parameters, interactions, and high orders at significant level of 5%. The models have demonstrated the importance of the R_s, UVI, U, RH, and TDS_F.

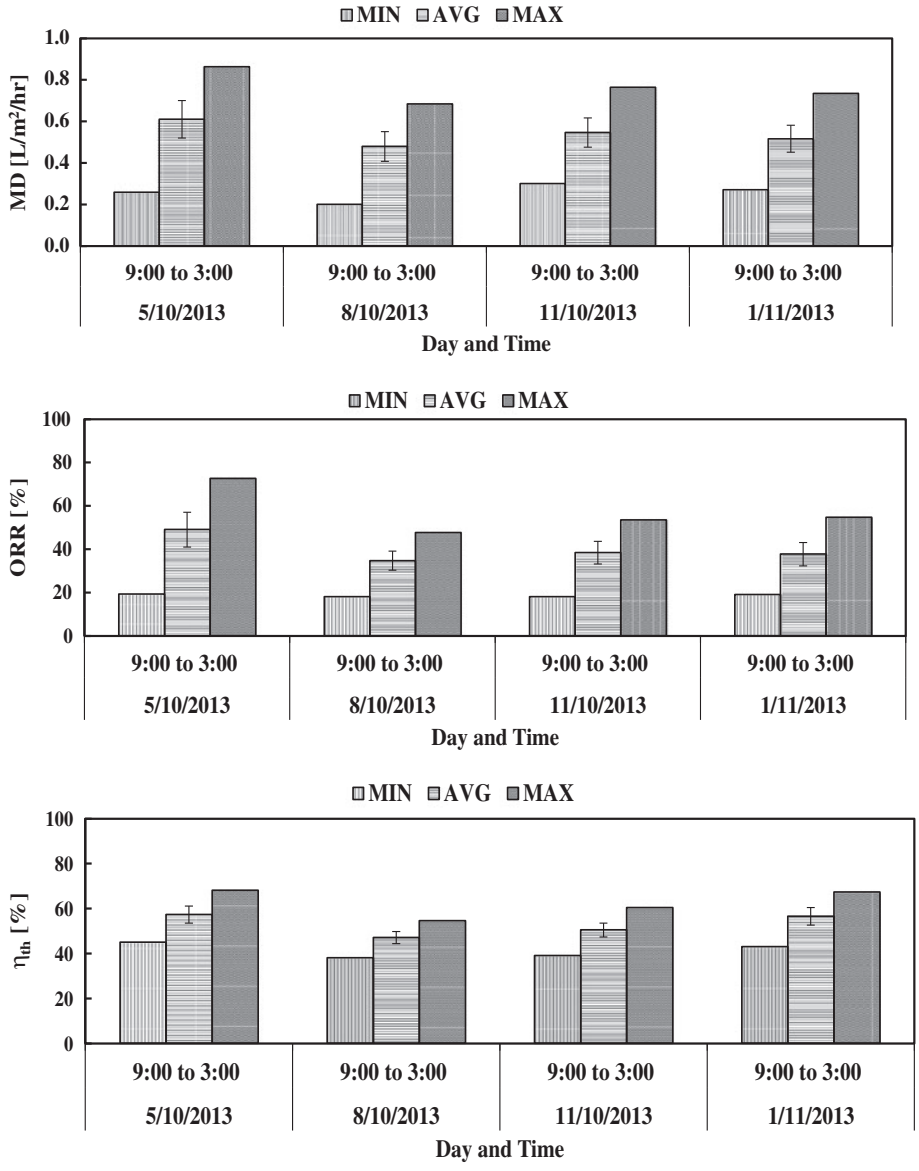

Fig. 7. Histograms for the MIN, AVG, and MAX of MD and ORR and η_{th} for the DW desalination process. The vertical error bar represents the standard deviation.

Moreover, it was revealed that UVI was the dominant parameter where the MD, ORR, and η_{th} were increased as the UVI increased. Probably, that was owing to the fact that increasing UVI resulted in an increase in T_B, which in turn increases the rate of evaporation, leading to an increase in MD, ORR, and η_{th}. The productivity of the system at high UVI trend to decrease that might be because of the formation of more fog in the solar still which reduces the condensation process of water vapor. According to the prediction model in Eq. (3), the predicted MD was plotted as a function of the measured MD. Fig. 10(a) shows a graph of 45° (1:1) for the predicted and measured data of the MD, where R^2 was 0.91. Eq. (4) shows that ORR increases as U decreases, which might be due to a decrease in the convective heat transfer coefficient (h). As the U decreases around the desalination system, less heat was lost to the surrounding and ORR increased. This agrees with the findings of Kalogirou [1], where he stated that the h mostly depends on the U. The interaction between RH and UVI had a positive effect on the recovery ratio, whereas the interaction with TDS_F had a negative effect on the η_{th} but was relatively small and appears at high concentrations. Additionally, Fig. 10(b) illustrated the good fit of the predicted and real values of ORR, where R^2

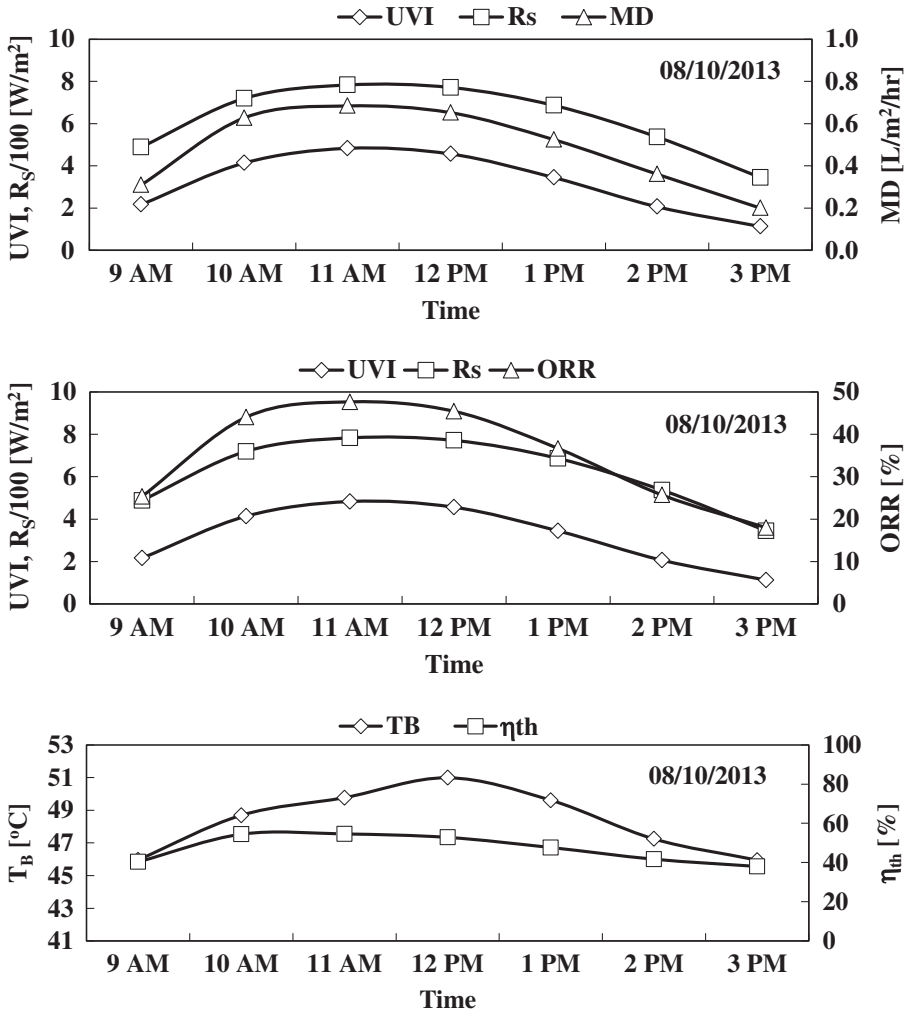

Fig. 8. Typical example of the changes of MD, ORR, and η_{th} with most affected parameters during one day of operation for DW.

was 0.939. Also, it should be noted that as the salt concentration of the feed (TDS_F) increased, productivity decreased. In general, η_{th} increased as TDS_F decreased and the reverse is true. It is clear that with low TDS_F, the rate of evaporation was higher, which might be attributed weak ionic bonds in the low concentration of salts compared to the medium or high concentration of salts in feedwater. The predicted and real η_{th} were illustrated in Fig. 10(c) to show goodness of fit.

For GW, the obtained models were displayed in Eqs. (6)–(8), with R^2 equal to 0.95, 0.96, and 0.95 for MD, ORR, and η_{th}, respectively.

$$MD = 0.030 + 10.494 \times 10^{-7} (R_S)^2 \quad (6)$$

$$ORR = 2.514 + 7.560 \times 10^{-5}(R_S)^2 \quad (7)$$

$$\eta_{th} = 23.4 + 0.117(R_S) - 5.67 \times 10^{-5}(R_S)^2 + 0.007(TDS_F \times TDS_B) - 0.847(TDS_F) - 1.316(T_o) + 0.016(T_o \times T_B) \quad (8)$$

Where the applicability of these equations was limited to the following ranges of the independent variables: R_s: 271.52–909.81 W/m^2; T_o: 34.72–43.75°C; T_B: 41.83–63.84°C; RH: 2.14–12%; TDS_F: 7.45–108.8 PPT and TDS_B: 6.71–108.87 PPT. The models showed the significance of the parameters as R_s, TDS_F, TDS_B, T_o, and T_B. The models revealed that R_s was the dominant parameter, either individual or in high orders, where

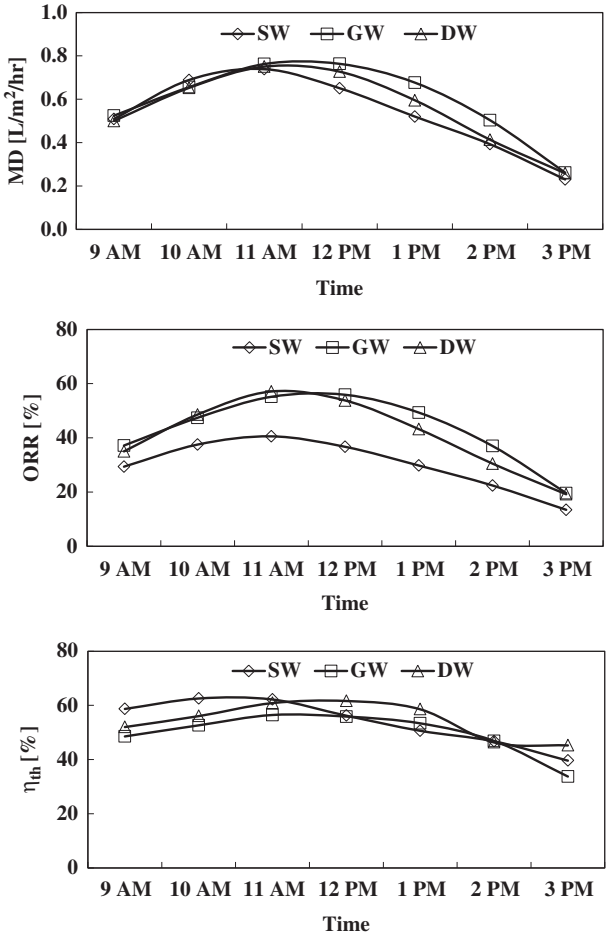

Fig. 9. Hourly average of MD, ORR, and η_{th} for each operation day for each type of water.

MD, ORR, and η_{th} increased as R_s increased. Perhaps that was because of the fact that increasing R_s resulted in an increase in the rate of evaporation, which in turn increases MD, ORR, and η_{th}. Manokar et al. [23] reported that the evaporation rate essentially depends on R_s. In accordance with the prediction model in Eq. (6), predicted MD was plotted as a function of measured MD. Fig. 11(a) shows the predicted and real data for MD; The R^2 was 0.95 which showed excellent agreement. Based on Eq. (7), ORR was predicted. Fig. 11(b) shows the relation between real and predicted data for ORR data from the statistical model. ORR showed the same trend as MD but with the highest R^2 at 0.96. Eq. (8) showed that R_s was the most important parameter that influenced η_{th}. This was consistent with Mohamed and El-Minshawy [44], who mentioned that the η_{th} value increases with the increase of R_s until it reaches a maximum value and then declines. Also, increasing TDS_F resulted in lower productivity. Overall, η_{th} decreased as TDS_F increased.

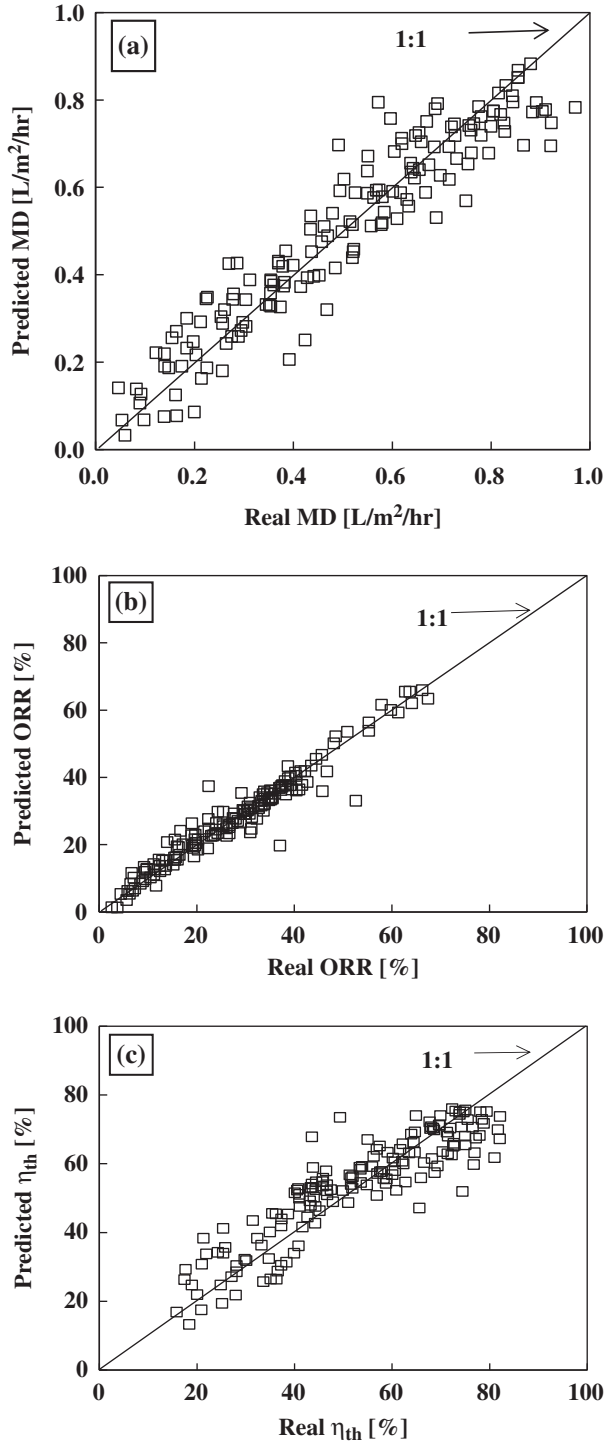

Fig. 10. Predicted vs. real MD (a), ORR (b), and η_{th} (c) values for SW.

It was clear that with decreasing TDS_F, the rate of evaporation increased, which as mentioned before it could be attributed to the weakness of ionic bonds for low concentrations of salts as compared to higher

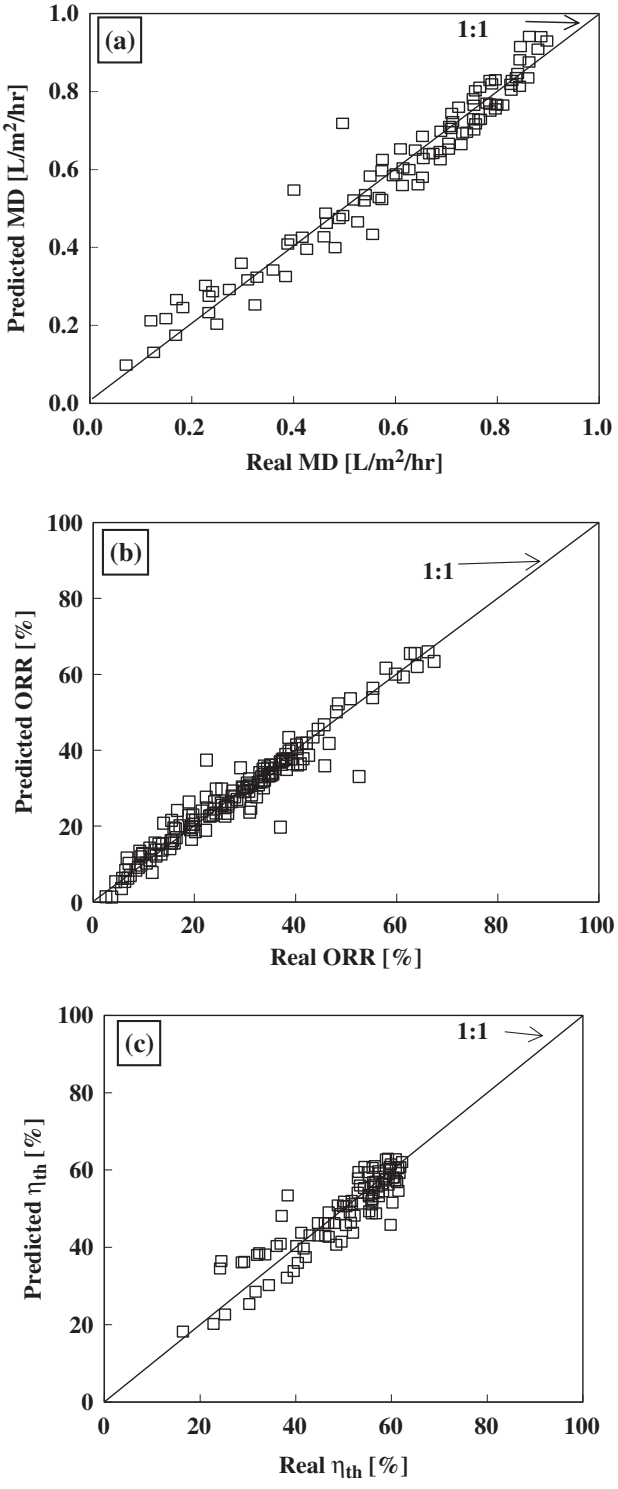

Fig. 11. Predicted vs. real MD (a), ORR (b), and η_{th} (c) values for GW.

concentrations of salts in feed stream. The interaction between TDS_F and TDS_B had a positive effect on η_{th} while the interaction between T_o and T_B had a positive effect on the η_{th}. The R_S^2, TDS_F, and T_o had a negative effect on η_{th} but it was relatively small. Fig. 11(c) presents the relation between real and predicted η_{th} data from the statistical model as indicated in Eq. (8) where the R^2 was 0.95.

For DW, the nonlinear regression analysis was utilized to find a reasonable set of empirical equations with significant constants that were presented in Eqs. (9)–(11) with R^2 equal to 0.91, 0.93, and 0.90 for MD, ORR, and $\eta_{th,}$ respectively.

$$MD = 0.141 + 0.003(UVI \times T_F) \quad (9)$$

$$ORR = 8.703 + 0.294(T_o \times UVI) \quad (10)$$

$$\eta_{th} = 43.242 + 0.128(T_o \times UVI) + 0.009(TDS_F^2) - 1.248(TDS_F) + 0.468(TDS_B) \quad (11)$$

Where the applicability of these equations was in the following ranges of the independent variables: T_o: 24.30–39.36 ℃;T_F: 29.39–42.75 ℃;UVI: 0.48–5.53;TDS_F: 4.71–99.43 PPT, and TDS_B: 7.3–108.3 PPT. The significance of all individual parameters, interactions, and high orders at a significant level of 5% has shown by the above models. The models have shown the importance of the parameters as the UVI, T_F, T_o, TDS_F, and TDS_B. From the models, UVI was the most in effect where the MD, ORR, and η_{th} were increased as the UVI increased. That was maybe owing to the fact that increasing UVI, leads to the increases in the rate of evaporation, thus MD, ORR, and η_{th} increase too. The predicted MD was plotted vs. the real MD as indicated in Fig. 12(a). In Eq. (9), it was cleared that the interaction between UVI and T_F had a positive effect on the MD. This is logical whereas increase each of UVI and T_F, the evaporation was increased which leads to the increased productivity. The predicted MD was validated well with that measured during the experimental period by the R^2 which was 0.91. According to the empirical equation Eq. (10), the interaction between UVI and T_O had a significant effect on the ORR. The relationship between the predicted values based on Eq. (10) and the real values was presented in Fig. 12(b) where R^2 was 0.93. In the case of the $\eta_{th,}$ it can be predicted by the statistical model in Eq. (11). Additionally, in Fig. 11, the relationship between the predicted and real of η_{th} values ($R^2 = 0.90$) was showed.

3.4. Physicochemical properties of the different water

During near-ZLD desalination of SW, GW, and DW, it is very important to know some of the

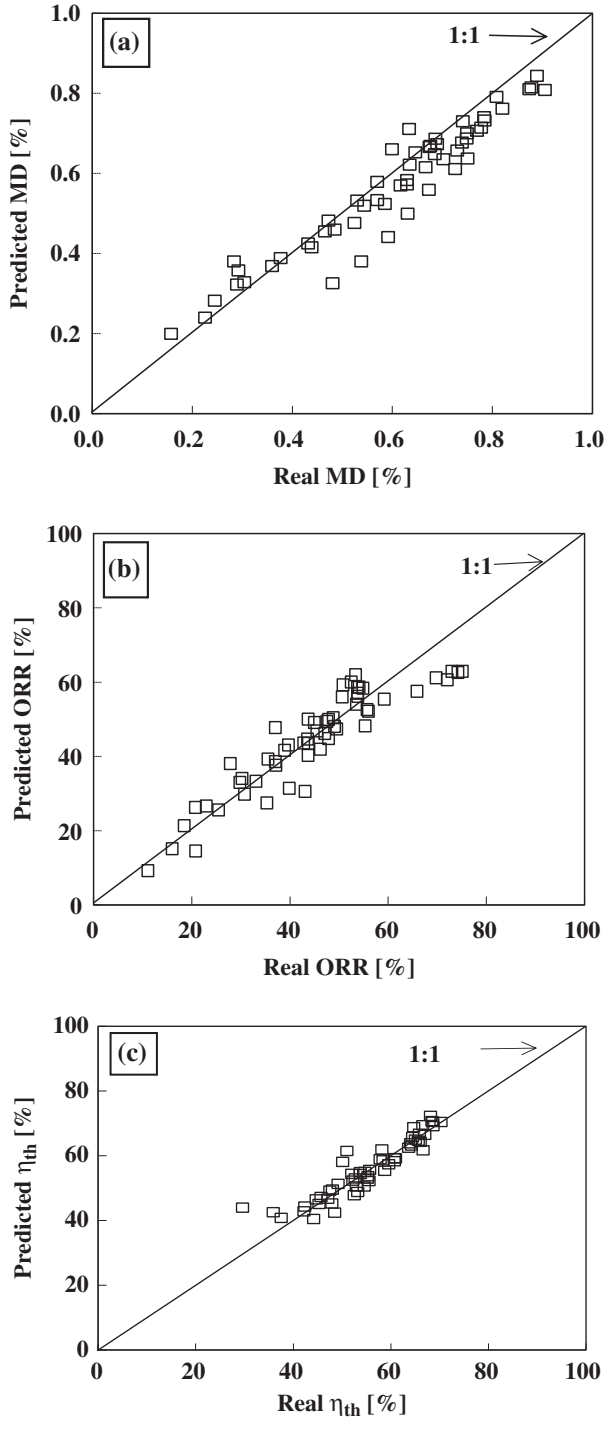

Fig. 12. Predicted vs. real MD (a), ORR (b), and η_{th} (c) values for DW.

physicochemical properties of the system streams, especially final brine water concentration and waste salt sludge, for proper handling and disposal. The average values and standard deviations of measured physicochemical properties (TDS, EC, pH, ρ, and color components) of the system streams were listed in Table 4.

The TDS and EC values of the raw SW before the desalination process were 41.40 PPT and 66.25 mS/cm, respectively. Because of the evaporation of water and the increase in the concentration during the process, the TDS and EC of the brine significantly increased and reached 131.1 PPT and 207.69 mS/cm, respectively, at the end of the process. The ρ of the raw SW before the desalination process was 1.0346 g/cm^3. The ρ of the final brine water was affected significantly by the increasing of TDS which was equal to 1.21350 g/cm^3 at the end of the process. The raw SW pH was 8.02, while the final brine pH was significantly less at 6.69. The drop in the pH of the brine was 16.6% compared with the pH of the raw SW. The color of the brine water was affected by the desalination process, with major changes in color occurring in the lightness component (L^*) where the changes in the other two components of color were limited. Persisting with the desalination process to reach the highest possible TDS resulted in a darker brine, where the L^* decreased as presented in Table 4.

On the other hand, for GW, TDS, and EC before the desalination process were 7.54 PPT and 11.93 mS/cm, respectively. Owing to the evaporation of water and increase in the concentration during the process, the TDS and EC of the brine significantly increased and reached 108.87 PPT and 174.19 mS/cm, respectively, at the end of the process. The ρ of the raw GW before the desalination process was 1.0065 g/cm^3. The ρ of the final brine water was affected significantly by the increasing of TDS, which equal to 1.21031 g/cm^3 at the end of the process. The pH of raw GW was 8.094, while the pH of final brine was significantly less at 6.89. The drop in the pH of the brine was 14.8% compared with the pH of the raw SW. The color of the brine water was affected by the desalination process, with color changes occurring in all components. Continuing the desalination process to reach the highest possible TDS resulted in a darker brine, where the L^* decreased as indicated in Table 4. The color component a^* (redness) increased as concentration increased. Furthermore, there was a noticeable increase in the values of the color component b^* toward yellowish.

Furthermore, for DW, TDS and EC before the desalination process were 4.71 PPT and 7.54 mS/cm, respectively. Due to the evaporation of water and increasing the concentration during the process, the TDS and EC of the brine were significantly increased and reached 108.30 PPT and 173.28 mS/cm, respectively, at the end of the process. The ρ of the raw DW before the desalination process was 1.0013 g/cm^3. The ρ of the final brine water was affected significantly by

Table 4
The TDS, EC, pH, density (ρ), and color components (L^*, a^*, b^*) of the system streams

Property	Fresh feedwater	Final brine water	Distilled water
SW			
TDS [PPT]	41.40 ± 0.10	131.1 ± 0.26	0.083 ± 0.06
EC [mS/cm]	66.25 ± 0.01	207.69 ± 0.01	0.1288 ± 0.05
pH	8.02 ± 0.03	6.69 ± 0.01	6.73 ± 0.16
ρ [g/cm^3]	1.0346 ± 0.00	1.2135 ± 0.00	0.9971 ± 0.00
L^*	69.85 ± 0.06	65.58 ± 0.01	70.28 ± 0.05
a^*	−0.690 ± 0.00	−0.697 ± 0.006	−0.700 ± 0.00
b^*	1.18 ± 0.01	1.19 ± 0.02	1.32 ± 0.01
GW			
TDS [PPT]	7.45 ± 0.01	108.87 ± 0.23	0.0174 ± 0.07
EC [mS/cm]	11.93 ± 0.01	174.19 ± 0.01	0.0278 ± 0.01
pH	8.094 ± 0.003	6.89 ± 0.01	7.07 ± 0.16
ρ [g/cm^3]	1.0065 ± 0.00	1.2103 ± 0.00	0.99740 ± 0.00
L^*	69.94 ± 0.02	34.36 ± 0.05	70.17 ± 0.02
a^*	−0.623 ± 0.01	17.22 ± 0.021	−0.643 ± 0.01
b^*	1.28 ± 0.03	47.04 ± 0.02	1.02 ± 0.01
DW			
TDS [PPT]	4.71 ± 0.01	108.30 ± 0.00	0.101 ± 0.00
EC [mS/cm]	7.54 ± 0.01	173.28 ± 0.01	0.041 ± 0.01
pH	8.09 ± 0.02	7.37 ± 0.01	7.69 ± 0.08
ρ [g/cm^3]	1.0013 ± 0.00	1.13732 ± 0.00	0.99680 ± 0.00
L^*	69.44 ± 0.03	53.23 ± 0.01	73.44 ± 0.48
a^*	−0.92 ± 0.01	8.74 ± 0.01	−0.84 ± 0.02
b^*	3.12 ± 0.04	51.74 ± 0.02	1.07 ± 0.01

the increasing of TDS where it was 1.13732 g/cm^3 at the end of the process. The pH of DW was 8.087, while the pH of the final brine was 7.37. The brine pH was significantly less than the pH of the raw DW. The drop in the pH of the brine was 8.87% compared with the pH of the raw DW. Also, as with SW and GW, the color of the brine water was affected by the desalination process. The changes in color occurred in all components. Persisting with the desalination process to reach the highest possible TDS resulted in darker brine, where the L^* decreased as shown in Table 4. The a^* increased by raising the concentration. Moreover, there was an obvious increase in the value of the b^*. According to WHO [45] and from the experimental results presented in Table 4 for the three types of water, the distilled water quality lies in the acceptable range. Additionally, it is considered excellent which makes it suitable for use in greenhouses, either in irrigation or in evaporative cooling.

3.5. Cost estimation

The total cost = Fixed cost + Variable cost, the fixed cost of solar still one meter is about 150 USD. As mentioned by Buongiorno et al. [46], variable cost equals 0.3 of a fixed cost per year. The anticipated solar still life is 10 years. Hence, the total cost = 150 + (0.3 × 150 × 10) = 600 USD. The average daily productivity is equal to about 5 L/m^2/d. Assume solar still operates 335 d/year. The total productivity throughout the solar still lifetime = 5 × 10 × 335 = 16,750 L. Consequently, the cost of one liter = 600/16,750 = 0.04 USD.

4. Conclusion

Solar energy can be used for desalination as an environmentally friendly, clean source of energy. Solar desalination of low quality water can contribute to meeting the increasing demand for water . This study shows that solar energy can be applied through solar stills to desalinate SW, groundwater, and agricultural DW. However, more investigation is necessary to determine how to optimize the process, especially in terms of distilled water productivity, recovery ratio, and thermal efficiency. The main outcome of this study is the evaluation of the application of solar energy to the desalination of water of different feedwater quality levels for near ZLD. The performance data associated with the solar still will bring new insights to system

analysis, design, and modeling and to the evaluation of the potential applications of the solar desalination to different types of low quality water in coastal and remote areas. Before the economic benefits of the solar desalination process can be evaluated, additional analyses and development are necessary. The data will assist in the scale up of the process to facilitate productive exploitation in the water supply field. A possible conclusion is that the solar desalination system's performance depends to a great extent on solar radiation, ultraviolet, and the TDS concentration of feedwater. The mathematical models of the performance parameters can be used to make accurate forecasts within the ranges specified in this study. More research work and a variety of emphases are recommended in order to investigate the quality of the product of the process (distillate water) and its utility for drinking, crop irrigation, and the greenhouse cooling process. This study gave preliminary indications of the effectiveness of the solar desalination of low quality water in achieving near-ZLD. Last of all, the desalination of high concentrations resulted in the problem of partial mixing between the brine stream and the distilled water. It will be necessary to modify the system's design to overcome this problem.

Acknowledgments

The project was financially supported by King Saud University, Vice Deanship of Research Chairs.

Symbols

DW	—	drainage water
EC	—	electrical conductivity (mS/cm)
GW	—	groundwater
MD	—	solar still productivity ($L/m^2/h$)
ORR	—	operational recovery ratio (%)
RH	—	relative humidity (%)
R_s	—	solar radiation (W/m^2)
SW	—	sea water
T	—	temperature (°C)
TDS	—	total dissolved solids (PPT)
T_o	—	air temperature (°C)
U	—	wind speed (km/h)
UVI	—	ultra violet index (–)
η_{th}	—	thermal efficiency (%)
ρ	—	density (g/cm^3)

Subscripts

B	—	brine
D	—	distillate
F	—	feedwater

References

[1] S.A. Kalogirou, Sea water desalination using renewable energy sources, Prog. Energy Combust. Sci. 31 (2005) 242–281.
[2] A. Tamimi, K. Rawajfeh, Lumped modeling of solar-evaporative ponds charged from the water of the Dead Sea, Desalination 216 (2007) 356–366.
[3] M.C. Giestas, H.L. Pina, J.P. Milhazes, C. Tavares, Solar pond modeling with density and viscosity dependent on temperature and salinity, Int. J. Heat Mass Transfer 52 (2009) 2849–2857.
[4] M. Karakilcik, K. Kıymaç, I. Dincer, Experimental and theoretical temperature distributions in a solar pond, Int. J. Heat Mass Transfer 49 (2006) 825–835.
[5] Z. Abdel-Rehim, A. Lasheen, Experimental and theoretical study of a solar desalination system located in Cairo, Egypt, Desalination 217 (2007) 52–64.
[6] R. Alnaizy, A.A. Aidan, Development of a renewable energy-based solution for saline waters desalinations, Proceedings of AIChE Annual Meeting, San Antonio, TX, March 21–25, 2010.
[7] J. Leblanc, A. Akbarzadeh, J. Andrews, H. Lu, P. Golding, Heat extraction methods from salinity-gradient solar ponds and introduction of a novel system of heat extraction for improved efficiency, Sol. Energy 85 (2011) 3103–3142.
[8] H. Khorasanizadeh, K. Mohammadi, M. Jalilvand, A statistical comparative study to demonstrate the merit of day of the year-based models for estimation of horizontal global solar radiation, Energy Convers. Manage. 87 (2014) 37–47.
[9] Y. Oren, E. Korngold, N. Daltrophe, R. Messalem, Y. Volkman, L. Aronov, M. Weismann, N. Bouriakov, P. Glueckstern, J. Gilron, Pilot studies on high recovery BWRO-EDR for near zero liquid discharge approach, Desalination 261 (2010) 321–330.
[10] F. Farahbod, D. Mowla, M.R. Jafari Nasr, M. Soltanieh, Experimental study of a solar desalination pond as second stage in proposed zero discharge desalination process, Sol. Energy 97 (2013) 138–146.
[11] A.P.R. Koppol, M.J. Bagajewicz, B.J. Dericks, M.J. Savelski, On zero water discharge solutions in the process industry, Adv. Environ. Res. 8 (2004) 151–171.
[12] A.M. Assiry, Application of ohmic heating technique to approach near-ZLD during the evaporation process of seawater, Desalination 280 (2011) 217–223.
[13] B.D. Stanford, J.F. Leising, R.G. Bond, S.A. Snyder, C.E. Isabel, I.S. Andrea, Inland desalination: Current practices, environmental implications, and case studies in Las Vegas, NV, Sustain. Sci. Eng. 2 (2010) 327–350 (Chapter 11).
[14] L. García-Rodríguez, Seawater desalination driven by renewable energies: A review, Desalination 143 (2002) 103–113.
[15] E. Chafik, A new seawater desalination process using solar energy, Desalination 153 (2002) 25–37.
[16] H.M.N. AlMadani, Water desalination by solar powered electrodialysis process, Renew. Energy 28 (2003) 1915–1924.
[17] L. Roca, M. Berenguel, L. Yebra, D.C. Alarco´n-Padilla, Solar field control for desalination plants, Sol. Energy 82 (2008) 727–786.

[18] A. El-Sadek, Water desalination: An imperative measure for water security in Egypt, Desalination 250 (2010) 876–884.
[19] D.C. Alarcón-Padilla, L. García-Rodríguez, J. Blanco-Gálvez, Design recommendations for a multi-effect distillation plant connected to a double-effect absorption heat pump: A solar desalination case study, Desalination 262 (2010) 11–14.
[20] G.M. Ayoub, L. Malaeb, Economic feasibility of a solar still desalination system with enhanced productivity, Desalination 335 (2014) 27–32.
[21] B. Bouchekima, Solar desalination plant for small size use in remote arid areas of South Algeria for the production of drinking water, Desalination 156 (2003) 353–354.
[22] A.Bhattacharyya, Solar stills for desalination of water in rural households, Int. J. Environ. Sustainability 2 (2013) 21–30.
[23] A. Muthu Manokar, K. Kalidasa Murugavel, G. Esakkimuthu, Different parameters affecting the rate of evaporation and condensation on passive solar still—A review, Renewable Sustainable Energy Rev. 38 (2014) 309–322.
[24] N.I. Santos, A.M. Said, D.E. James, N.H. Venkatesh, Modeling solar still production using local weather data and artificial neural networks, Renew. Energy 40 (2012) 71–79.
[25] S.M.A. Moustafa, G.H. Brusewitz, D.M. Farmer, Direct use of solar energy for water desalination, Sol. Energy 22 (1979) 141–148.
[26] Y.H. Zurigat, M.K. Abu-Arabi, Modelling and performance analysis of a regenerative solar desalination unit, Appl. Therm. Eng. 24 (2004) 1061–1072.
[27] V. Dimri, B. Sarkar, U. Singh, G.N. Tiwari, Effect of condensing cover material on yield of an active solar still: An experimental validation, Desalination 227 (2008) 178–189.
[28] T.V. Arjunan, H.S. Aybar, N. Nedunchezhian, Effect of sponge liner on the internal heat transfer coefficients in a simple solar still, Desalin. Water Treat. 29 (2011) 271–284.
[29] S. Shanmugan, B. Janarthanan, J. Chandrasekaran, Performance of single-slope single-basin solar still with sensible heat storage materials, Desalin. Water Treat. 41 (2012) 195–203.
[30] A.A. Al-Karaghouli, W.E. Alnaser, Experimental comparative study of the double basin solar stills, Appl. Energy 77 (2004) 317–325.
[31] K. Kalidasa Murugavel, K. Srithar, Performance study on basin type double slope solar still with different wick materials and minimum mass of water, Renew. Energy 36 (2011) 612–620.
[32] A.A. El-Sebaii, Thermal performance of a triple-basin solar still, Desalination 174 (2005) 23–37.
[33] A. Ahsan, M. Imteaz, R. Dev, H.A. Arafat, Numerical models of solar distillation device: Present and previous, Desalination 311 (2013) 173–181.
[34] F.F. Tabrizi, M. Dashtban, H. Moghaddam, Experimental investigation of a weir-type cascade solar still with built-in latent heat thermal energy storage system, Desalination 260 (2010) 248–253.
[35] N. Syuhada, A. Ahsan, U.A. Thomas, M. Imteaz, A.H. Ghazali, A low cost solar still for pure water production, J. Food Agric. Environ. 11 (2013) 990–994.
[36] T. Arunkumar, A. Ahsan, Effect of water flow on concentrator coupled hemispherical basin solar still, Int. J. Appl. Nat. Sci. 2 (2013) 23–28.
[37] A.A. Madani, Zero-discharge direct-contact freezing/solar evaporator desalination complex, Desalination 85 (1992) 179–195.
[38] M.C. Pereira, J.F. Mendes, P. Horta, N. Korovessis, Final design of an advanced solar dryer for salt recovery from brine effluent of an MED desalination plant, Desalination 211 (2007) 222–231.
[39] F. Farahbod, D. Mowla, M.R. Jafari Nasr, M. Soltanieh, Experimental study of forced circulation evaporator in zero discharge desalination process, Desalination 285 (2012) 352–358.
[40] K.M. Sassi, I.M. Mujtaba, Simulation and optimization of full scale reverse osmosis desalination plant, Comput. Aided Chem. Eng. 28 (2010) 895–900.
[41] O.O. Badran, M.M. Abu-Khader, Evaluating thermal performance of a single slope solar still, Heat Mass Transfer 43 (2007) 985–995.
[42] A.E. Kabeel, M.H. Hamed, Z.M. Omara, Augmentation of the basin type solar still using photovoltaic powered turbulence system, Desalin. Water Treat. 48 (2012) 182–190.
[43] A.M. Radhwan, Transient performance of a steeped solar still with built-in latent heat thermal energy storage, Desalination 171 (2004) 61–76.
[44] A.M.I. Mohamed, N.A. El-Minshawy, Theoretical investigation of solar humidification dehumidification desalination system using parabolic trough concentrators, Energy Convers. Manage. 52 (2011) 3112–3119.
[45] WHO, Guidelines for Drinking-water Quality, third ed., World Health Organization, Geneva, 2004.
[46] J. Buongiorno, L.W. Hu, G. Apostolakis, R. Hannink, T. Lucas, A. Chupin, A feasibility assessment of the use of nanofluids to enhance the in-vessel retention capability in light-water reactors, Nucl. Eng. Des. 239 (2009) 941–948.